Tracking Functional Network Connectivity Dynamics in the Elderly

Kaichao Wu [1,2]**, Beth Jelfs** [3,*]**, Seedahmed S. Mahmoud** [1]**, Katrina Neville** [2]**,**

John Q. Fang [1,*]

[1]*Department of Biomedical Engineering, College of Engineering, Shantou University, Shantou, P.R.China*

[2]*School of Engineering, RMIT University, Melbourne, Australia.*

[3]*Department of Electronic, Electrical and Systems Engineering, The University of Birmingham, Birmingham, UK.*

Correspondence*:
John Q. Fang
qiangfang@stu.edu.cn

Beth Jelfs
b.jelfs@bham.ac.uk

2 **ABSTRACT**

3   Functional magnetic resonance imaging (fMRI) has shown that ageing disturbs healthy brain
4 organization and functional connectivity. However, how this age-induced alteration impacts
5 dynamic brain function interaction has not yet been fully investigated. Dynamic function network
6 connectivity (DFNC) analysis can produce a brain representation based on the time-varying
7 network connectivity changes, which can be further used to study the brain ageing mechanism
8 for people at different age stages. Hence, this presented investigation examined the dynamic
9 functional connectivity representation and its relationship with brain age for people at an elderly
10 stage as well as in early adulthood. Specifically, the resting-state fMRI data from the University
11 of North Carolina cohort of 34 young adults and 28 elderly participants were fed into a DFNC
12 analysis pipeline. This DFNC pipeline forms an integrated dynamic functional connectivity (FC)
13 analysis framework, which consists of brain functional network parcellation, dynamic FC feature
14 extraction, and FC dynamics examination. The statistical analysis demonstrates that extensive
15 dynamic connection changes in the elderly concerning the transient brain state and the method
16 of functional interaction in the brain. In addition, various machine learning algorithms have been
17 developed to verify the ability of dynamic FC features to distinguish the age stage. Results
18 show that the fraction time of DFNC states has the highest performance, which can achieve a
19 classification accuracy of over 88% by a decision tree. Furthermore, the dynamic FC alteration
20 has been found to be correlated with mnemonic discrimination ability and could have an impact
21 on the balance of functional integration and segregation.

22 **Keywords: Ageing, Dynamic functional network connectivity, Graph theory, Mnemonic Discrimination Ability, Functional integration**

23 **and segregation**

1 INTRODUCTION

24 Ageing has a profound influence on the brain's structure and function at both local and global scales. These
25 effects are responsible for decreased mental and physical fitness (Cole et al., 2018) and increased risk of
26 neurodegenerative diseases such as Alzheimer's disease (Abbott, 2011), or Parkinson's disease (Reeve et al.,
27 2014) (Dennis and Thompson, 2014). Functional magnetic resonance imaging (fMRI) is a powerful and
28 efficient, accessible and non-invasive tool, which has been extensively used to reveal neural mechanisms
29 engaged in the normal ageing process. It has also contributed greatly to elucidating the role that ageing
30 plays in the decline of brain function (e.g., the cognitive (Uddin et al., 2017) or motor function (Thomason
31 et al., 2008)). More precisely, resting-state fMRI studies have frequently reported altered connectivity both
32 within-network and between-network. In human ageing the findings encountered include: the functional
33 connectivity (FC) decreases within higher-order networks and segregation of networks diminishes with
34 advancing age. For example, within the default network, the salience network, and the frontoparietal
35 control network, FC has been reported to be reduced (Fjell et al., 2016; Grady et al., 2016). This FC
36 alteration could be a sign of neural or functional network reorganisation, however, these findings rely
37 on the static functional network connectivity analysis (SFNC). One potential limitation of SFNC is the
38 theoretical assumption that the FC exhibits a constant state during a rest MRI period. This means that the
39 fine-grained temporal evaluation of resting state has been neglected, and the flexibility of the functional
40 network reorganisation cannot be assessed.

41   Recently, with the advances in understanding of the temporal resolution of resting-state fMRI, the interest
42 in how normal human ageing affects the time-varying or dynamic functional network connectivity (DFNC)
43 has increased (Calhoun et al., 2014). For instance, the loss or decline of FC dynamics has been wildly
44 found in the elderly adult group (Chen et al., 2017; Schaefer et al., 2014). This temporal variation of FC
45 reflects the network flexibility necessary for brain function response, which fits our intuitive perception of
46 the elderly who have the loss of physical flexibility. In contrast with SFNC, an advantage of DFNC is that
47 it allows the fluctuation of FC, within or between the brain functional networks, over short periods to be
48 observed. Identification of the FC fluctuation patterns allows the brain's FC state profile to be identified.
49 Following which, features characterizing the FC dynamics, such as the transition trajectories between
50 distinct brain states (Allen et al., 2014; Vidaurre et al., 2021) can then be used to interpret brain behaviours.

51   Given such a capacity, DFNC has been increasingly applied to brain ageing. For instance, the DFNC
52 method has demonstrated that the FC dynamics degenerate in normal ageing. This degeneration is reflected
53 by the lower switching rate between brain states within salience network (Snyder et al., 2021) and
54 default network (Xia et al., 2019), as well as by the decreased connectivity flexibility in the right middle
55 frontal gyrus (Yin et al., 2016). The FC dynamics has also been demonstrated to correlate with cognitive
56 ability (Xia et al., 2019). Studies using DFNC methods have revealed other opinions regarding dynamic FC.
57 For example, FC dynamics is usually characterized by the switching rate of connectivity states, which is
58 defined as the rate at which a state transitions between potential functional brain states over a certain period.
59 However, in a study investigating the human brain across the lifespan, for example, the switching rate of
60 brain state was observed to have no difference between different age groups (Viviano et al., 2017). These
61 distinct results are possibly due to differences in the implementation method and the data samples. While
62 the results are not consistent, all these collected findings imply that the DFNC analysis is a promising
63 method for providing insight into human ageing neuromechanisms from multiple views and means.

64   Therefore, in this research, we explore the brains of two age-different groups with the DFNC method, to
65 track the FC dynamics in the elderly over the MRI scan and to investigate the relationship between dynamic
66 FC and age. Overall, we expect that the study of DFNC can reveal and track the change in flexibility of

67 function coordination and interaction in the elderly, and this alteration can facilitate brain age estimation at
68 an individual level. This research also has the potential to form the basis for further investigations which
69 may provide a deeper understanding of brain changes and ageing. This could offer clues to the relationship
70 between brain maturity and brain behaviors as well as age-induced diseases.

71 Specifically, the resting-state functional MRI data from 34 younger adults aged 19 to 22 and 28 elderly
72 adults aged 60 to 80 have been tested by an implemented DFNC analysis pipeline. The fMRI data is used
73 to identify the intrinsic connectivity networks (ICNs), from which the brain states are estimated and the
74 dynamic features extracted. The alterations in FC dynamics caused by ageing were examined, and the
75 power of dynamic features in individual age prediction was evaluated in this framework. In addition, we
76 have also discussed the relationship between dynamic features and mnemonic discrimination ability and
77 the dynamic balance of functional integration and segregation in healthy ageing.

2 MATERIALS AND METHODS

2.1 fMRI acquisition

79 Resting-state scans were obtained from the University of North Carolina samples at Greensboro[1] after
80 request, without any rights conflicts. The participants were 28 elderly adults (61–80 years old, mean age $\pm$
81 standard: 69.82$\pm$5.64; 20 female) and 34 young (18–32 years old, mean age $\pm$ standard deviation(SD):
82 22.21$\pm$3.65; 20 female). Participants were instructed to lie motionlessly in the scanner and stay awake with
83 their eyes open. All functional images were collected using a Siemens Trio 3.0T scanner with a 16-channel
84 head coil and the following recording parameters: 32 slices with 4.0 mm thickness and no skip, time of
85 echo = 30 ms; time of repetition (TR) = 2000 ms; flip angle = 70, field of view = 220 mm, matrix size = 74
86 $\times$ 74 $\times$ 32 voxels, 300 volumes in 10 minutes.

2.2 fMRI data preprocessing

88 The data for each participant has 300 measurements recorded over 10 minutes. The first five volumes of
89 each scan were discarded to allow for magnetic stability and thus to generate a steady blood oxygenation
90 level-dependent activity signal. The functional data was then processed with the following steps:

91 1. Realignment to correct head motion (see Section 2.3 for verification details).
92 2. Slice time correction.
93 3. Outlier identification.
94 4. Normalization (normalize to 3 mm MNI space using a templates from the SPM software
95   package (Ashburner and Friston, 2005)).
96 5. Spatial smoothing with a Gaussian kernel of 8 mm full-width at half-maximum (FWHM).

97 The processing pipeline was executed using the CONN toolbox (Whitfield-Gabrieli and Nieto-Castanon,
98 2012).

2.3 Verification of head motion correction

100 To verify there was no significant head movement in the data, for each participant the individual mean
101 and maximum framewise displacements (FD) (Power et al., 2012) were calculated. As the participants
102 with large outlier scans have been removed from the raw data, none of the available participants had head

---

[1] https://openneuro.org/datasets/ds003871/versions/1.0.2

103 motion greater than 0.5 mm. No significant group difference in FD was observable when comparing the
104 final sample of 28 old adults and 34 young adults (p = 0.92).

105 **2.4 Static functional network connectivity analysis**

106 To assess static connectivity, pairwise Pearson correlations were computed over the entire timeseries
107 and then Fisher's Z-transformed. Group ICA-based was used to produce brain parcellations according to
108 the same procedure as described in Section 2.5.1. This calculation resulted in correlation coefficients per
109 participant, which represent the connectivity strength between the given ICNs. Then, the static connectivity
110 matrices were averaged across the young and elderly adult groups.

111 The difference in static connectivity between the young and elderly groups was evaluated through a
112 two-sample t-test (a significance level of $p < 0.05$). The correction for multiple comparisons was applied
113 using false discovery rate (FDR)-correction to determine statistical significance at $p < 0.05$ (Benjamini
114 and Hochberg, 1995).

115 **2.5 Dynamic functional network connectivity analysis**

116 Figure 1 shows the framework of our DFNC approach. Specifically, there are five main steps in this
117 pipeline:

118 1. Group independent component analysis (ICA) parcellation for intrinsic connectivity network (ICN)
119   recognition,
120 2. Sliding window cross-correlation,
121 3. Clustering analysis for brain state estimation,
122 4. Dynamic feature extraction,
123 5. FC dynamics examination via statistics and machine learning tests.

124 Details of each step are provided in the following sections.

125 2.5.1 Step 1: Group independent component analysis parcellation

126 Group ICA was performed in order to parcellate the brain into various functional networks. Following
127 the recommendations from previous studies (Allen et al., 2014; Xia et al., 2019; Abrol et al., 2017), the
128 number of components that can functionally parcellate the brain was predefined at 100. The configuration
129 for the group information-guided ICA algorithm was developed according to the detailed description
130 provided by (Salman et al., 2019). In particular, we adopt the two-stage Principal Component Algorithm
131 (PCA) to preserve the components that account for the most variance. In the first stage, each participants'
132 functional data was decomposed into 120 principal components (PCs), and the PCs of all participants
133 were concatenated across time and then further reduced to 100 in the second stage. Finally, the infomax
134 algorithm, from the ICASSO software package (Himberg and Hyvarinen, 2003), was used with 20 repeats
135 to find steady independent components (ICs). After back reconstruction, the participant-specific spatial
136 maps and corresponding time courses can be obtained. Three methods were employed to detect the ICNs
137 from potential functional networks:

138 **(1)** The spatial activation maps from the ICs were visually inspected to identify if they match the large-
139   scale functional network locations from previous studies (Kim et al., 2017; Di and Biswal, 2015) and
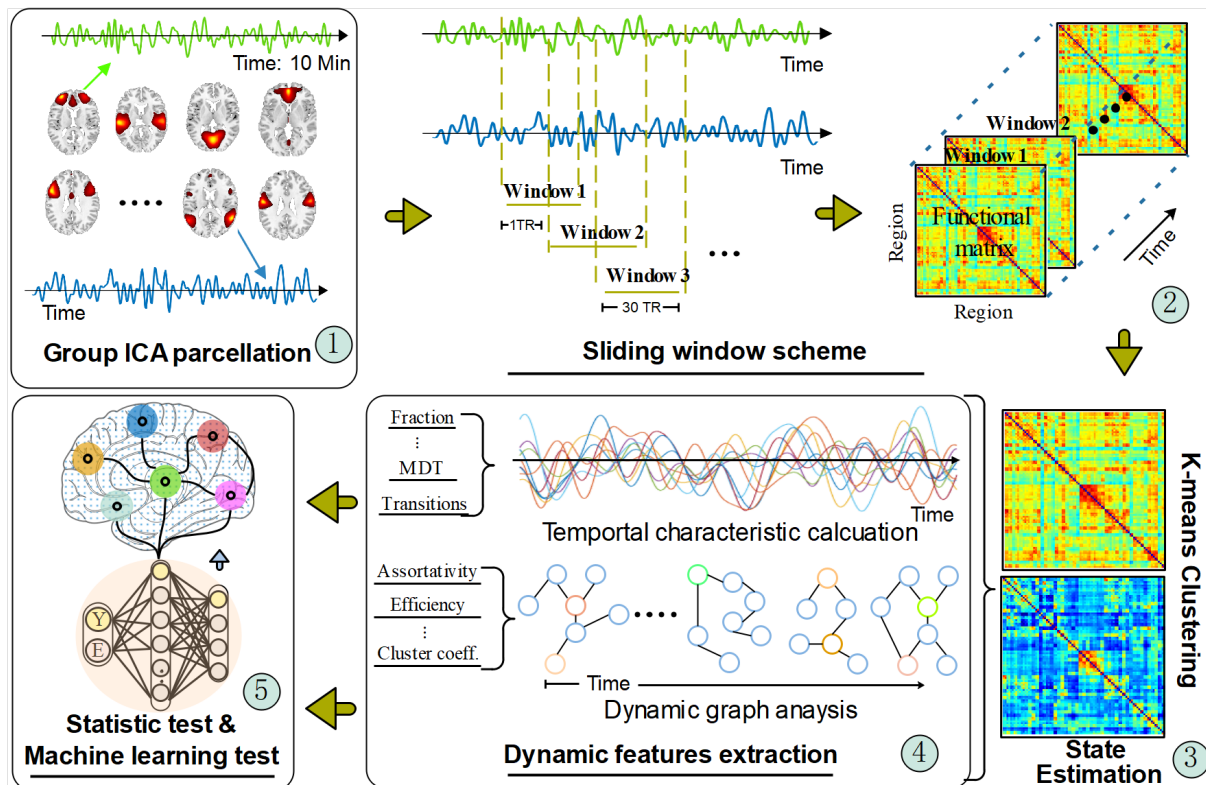140   anatomical brain regions.

Figure 1. The dynamic functional connectivity analysis pipeline. The timeseries signal was extracted from the network regions recognized from the group ICA parcellation method. Then, the regional timeseries were decomposed with a sliding window scheme for a time-varying function network connectivity(FNC) estimation. Those FNC matrixes were fed into a clustering algorithm to obtain different transient brain states by forming a cluster centroid. After that, two types of dynamic features were calculated based on the acquired transient states and temporal signals. Finally, statistical and machine learning methods were applied to verify the extracted dynamic FC features.

(2) The multiple regression method was used to select ICs whose spatial pattern matches with the existing functional networks template given by:

$$Y = \beta_1 X_1 + \beta_2 X_2 + \cdots + \beta_n X_n + \varepsilon, \tag{1}$$

where Y is the collection of the spatial vector of template ICNs, X_i represents the spatial vector of the i-th IC and β is the regression coefficient. The regression analysis is used to select the ICs closest to the functional network template spatially (the first rank of β), and the calculation is done by least-squares estimation.

(3) The power spectrum of the ICs was checked to see if it follows a low-frequency peak and a high-frequency steady pattern (the time courses of ICs are characterized by high dynamic range) (Griffanti et al., 2017).

Following the practice presented in (Bonkhoff et al., 2020; Tu et al., 2019), before passing the ICNs to the subsequent steps of the DFNC pipeline, additional post-processing of the time courses of all included ICNs was performed. The post-processing involved (a) linear, quadratic, and cubic detrending, (b) regressing out motion parameters (six realignment parameters and their first temporal derivatives), (c) low-pass filtering with a high-frequency cut-off of 0.15 Hz (to retain only BOLD-related signal fluctuations (Calhoun et al.,

155 2001)), and (d) despiking using 3D despike. These actions ensure artifact noise has minimal impact on the
156 signal analysis.

2.5.2 Step 2: Sliding window cross-correlation scheme

158 In the second step a sliding window is used to segment the timeseries of the ICNs into sub-fragments.
159 For each time window the correlations between the ICNs during that window were calculated. There
160 is no consensus in terms of the window size and the length of the sliding step. However, prior studies
161 provide evidence that a window size between 30s and 60s enables successful estimation of DFNC giving an
162 appropriate balance between accurate calculation of the correlation and the ability to detect time variations
163 in the ICN timeseries (Liégeois et al., 2016; Preti et al., 2017; Hindriks et al., 2016). Thus, in our experiment,
164 we opted for the common parameter settings, where the width of the window is 22 TR time (Kim et al.,
165 2017; Bonkhoff et al., 2020), windows were convolved with a Gaussian of $\sigma = 3$ TR to smooth the transition
166 between windows (Allen et al., 2014), and the window shifted with a step of 1 TR (Bonkhoff et al., 2020; Tu
167 et al., 2019). The window cross-correlation produced 273 correlation matrices, representing the fluctuation
168 of functional connectivity between the identified ICNs. These matrices are Fisher's Z transformed before
169 being passed to step 3 for clustering analysis.

2.5.3 Step 3: Clustering analysis for brain state estimation

171 Recurrent or repeating connectivity patterns in an fMRI scan are known as dynamic brain states. To
172 identify these brain states clustering is performed using the k-means based clustering algorithm. The
173 distance between clustering points was computed using the Manhattan distance (i.e., the "city-block"),
174 which is the distance metric recommended for high-dimensional-space clustering (Aggarwal et al., 2001).
175 The number of clusters is automatically computed by maximizing the ratio of within-cluster distance
176 and between-cluster distance, and the optimal candidate is then manually estimated using the elbow
177 method (Allen et al., 2014; Bonkhoff et al., 2020). For each subject the correlation matrices from step 2
178 were grouped into different clusters according to the distance from the clustering centroid. This results in
179 state labels for each of the time windows which are used in the dynamic feature calculations in the next
180 step in order to investigate the difference between the young and elderly adult groups.

2.5.4 Step 4: Dynamic feature extraction

182 Next, the FC temporal characteristic evaluation as well as the dynamic graph analysis were performed.
183 Following (Allen et al., 2014; Bonkhoff et al., 2020), using the state labels, four FC temporal characteristics
184 were calculated as features for the between-group difference: (i) state fraction: the percentage of the total
185 number of FC windows for one subject which take the given state; (ii) mean dwell times: the mean time
186 a subject spent in a state without switching to another one; (iii) number of transitions: how many times
187 a subject changed states; and (iv) transition probability matrix: the transition likelihood between the k
188 connectivity states.

189 The rationale behind the dynamic graph analysis is that, with the FC potentially fluctuating with each
190 time window, so too the topological structure of the graph can vary. For the dynamic graph analysis, as
191 shown in step 4 in Figure 1, the ICNs were defined as the nodes in the graph and the FC between them as
192 the edges, thus for each participant a graph is obtained for each time window. To define the adjacency of the
193 nodes a threshold can be applied to the edges in the graph to produce an undirected and binary adjacency
194 matrix. However, as the topological structure is not constant within one graph if using different network
195 thresholds, the network sparsity method has been adopted in our experiment to avoid the bias of unstable
196 measures in between-group dynamic feature comparison (Kim et al., 2017; Xia et al., 2019; Zhang et al.,

197 2011; Rashid et al., 2021). Similar to prior studies (Hashmi et al., 2017; Tu et al., 2019; van den Heuvel
198 et al., 2017), 10 thresholds ranging from 0.05 to 0.50 with a step of 0.05 were used to obtain the sparse
199 network. Each threshold produced an adjacency matrix for each DFNC matrix.

200 Having obtained the adjacency matrices then, graph theory was applied to investigate the topological
201 organization of the DFNC state and the series of graphs. Specifically, we use 12 graph metrics to measure
202 the graph characteristics and dynamics during the fMRI scan. For example, network efficiency, measures
203 how efficiently a node exchanges information or communicates with other nodes within a network. The
204 other selected metrics include assortativity, global and local efficiency, and synchronisation, which depict
205 a brain function network's resilience, segregation, and integration. Detailed definitions of these graph
206 metrics and their formulas are listed in Table 1 in the Supplemental Materials: Appendix 1. To balance the
207 sparsity selection for the sequence of thresholds, the area under the curve (AUC) for the metric values was
208 computed. Then, the AUC was utilised as a graph feature for further analysis.

2.5.5 Step 5: Statistics and machine learning tests

210 The final step in the pipeline conducts statistical testing to examine the results. To obtain robust and
211 reliable results on ageing-related variations within and between groups, a non-parametric permutation test
212 with 5000 randomizations was implemented for all of the dynamic features produced in the DFNC analysis
213 pipeline. The difference in the means of the distributions yielded after the 5000 random permutations
214 served as the t statistic. In addition, we investigated the presence of the distinct transient brain states
215 across different age groups by performing a two-sample t-test. All statistical results were corrected by false
216 discovery rate (FDR) for multiple comparison correction with a significance level of $p < 0.05$.

217 Meanwhile, nine machine learning algorithms were implemented to examine the power of the dynamic
218 features to predict the age of an individual. These algorithms were exploited to learn a mapping from the
219 raw fMRI space, $\mathcal{X}$, to the age distribution of participants, $\mathcal{Y}$. That is: $\Phi : \mathcal{G}(\mathcal{X}) \rightarrow \mathcal{Y}$ given the fMRI
220 scan collection of training samples $\mathcal{T} = \left\{ (x_n, y_n) \right\}_{n=1}^{N}$. Here, N is the number of training sample scans,
221 $x_n \in \mathcal{X}$ is the input scan and $y_n \in \mathcal{Y}$ is the associated age label indicating if the participant is an elderly
222 adult. $\mathcal{G} = \{g_i\}_{i=1}^{V}$ is the function extracting dynamic FC features, and V is the number of features.

223 These algorithms were all implemented using the sklearn python package. For the 6 methods listed in
224 Table 1 the default setup with the given parameters was used. In addition, we developed a neural network
225 method using Keras's deep learning package. Considering our small sample data size could cause problems
226 with over-fitting in the training phase for complicated network structures, a 2-layer forward neural network
227 (FNN) was developed. The first and second layers of the neural network compose of 256 and 2 neurons
228 (corresponding to the number of age categories.). At the end of the first and second layers, there is a tanh
229 and sigmoid activation function to learn the non-linear mapping relationship. The model is trained by
230 minimising the loss function:

$$L_{loss} = \frac{1}{N} \sum_i -\left[y_i \cdot \log(p_i) + (1 - y_i) \log(1 - p_i) \right], \tag{2}$$

231 where p_i is the predicted probability. Finally, we test two ensemble fusion-based methods: one is
232 Adaboost (Hastie et al., 2009), and the other one is Voting (Ruta and Gabrys, 2005). Both algorithms try to
233 promote prediction performance by weighting multiple embedded estimators. In the Adaboost method, the
234 default setup was opted for. In the voting method, the ensemble rule was set to be "hard", which means that
235 the predicted class labels for majority voting will be the final prediction results.

Table 1. Machine learning algorithms and their parameters.

Algorithm	Parameters
Nearest Neighbors	number of neighbors = 2
Linear SVM	regularisation parameter = 0.025
RBF SVM	same as Linear SVM
Gaussian Process	default
Decision Tree	depth = 5
Random Forest	number of neighbors = 5, number of estimators = 10

The dynamic feature output by g_i was singly fed into these machine learning methods to examine whether the ageing group classification facilitates dynamic classification. In addition, we have also cascaded the outputs of $\mathcal{G}\left(\mathcal{X}\right)$ together to examine if the concatenated dynamic feature can promote the performance.

3 RESULTS

3.1 Intrinsic connectivity networks

Of the 100 ICs identified by the group ICA, 40 ICs were identified as noise components and then discarded. The remaining 60 components were finally identified as ICNs. The 60 ICNs were assigned to one of six domains that have been widely studied in normal ageing (Snyder et al., 2021; Xia et al., 2019) (Figure 2): subcortical domain (SC), auditory domain (AUD), visual domain (VIS), sensorimotor domain (SM), cognitive control domain (CC), and default mode domain (DMN). The detailed component labels and peak coordinates of each ICN have been provided in the Supplementary Material:Appendix 2.

3.2 Static functional network connectivity analysis

Figure 3 shows the static functional network connectivity aggregated over the entire scanning time series using the group ICA method. The red colour indicates a positive correlation, and the blue colour represents a negative correlation between functional spatial regions. With the static functional network connectivity, we observed strong intra-domain connectivity, i.e., connectivity within the DMN, SMN, VIS, and AUD domains was positively correlated. In contrast, the inter-domain connectivity was comparably low, where the functional regions in the 6 domains were either independent of each other or negatively connected. This phenomenon was particularly obvious for the SC domain, where the connectivity with the other 5 domains was nearly all negative. Within the SC domain, the brain areas also exhibit negative connectivity.

Further reviewing the difference in connectivity from the elderly group and the younger using a two-sample t-test, 193 connectivity pairs show significantly altered between-network connectivity components. The significant alterations in ICNs have been denoted with an asterisk in Figure 3(A), from which we can see that these alterations are mainly related to the CC domain. Post t-tests, contrasting elderly adults and younger controls, reveals ageing-induced reduced connectivity ($p < 0.05$, FDR-corrected). From Figure 3(B), we can see only the connectivity between SM and CC domains was left after post t-tests in group ICA ($p < 0.05$, FDR-corrected). This result shows consistency with the studies that show higher connectivity between the somatosensory and control network (Geerligs et al., 2015).
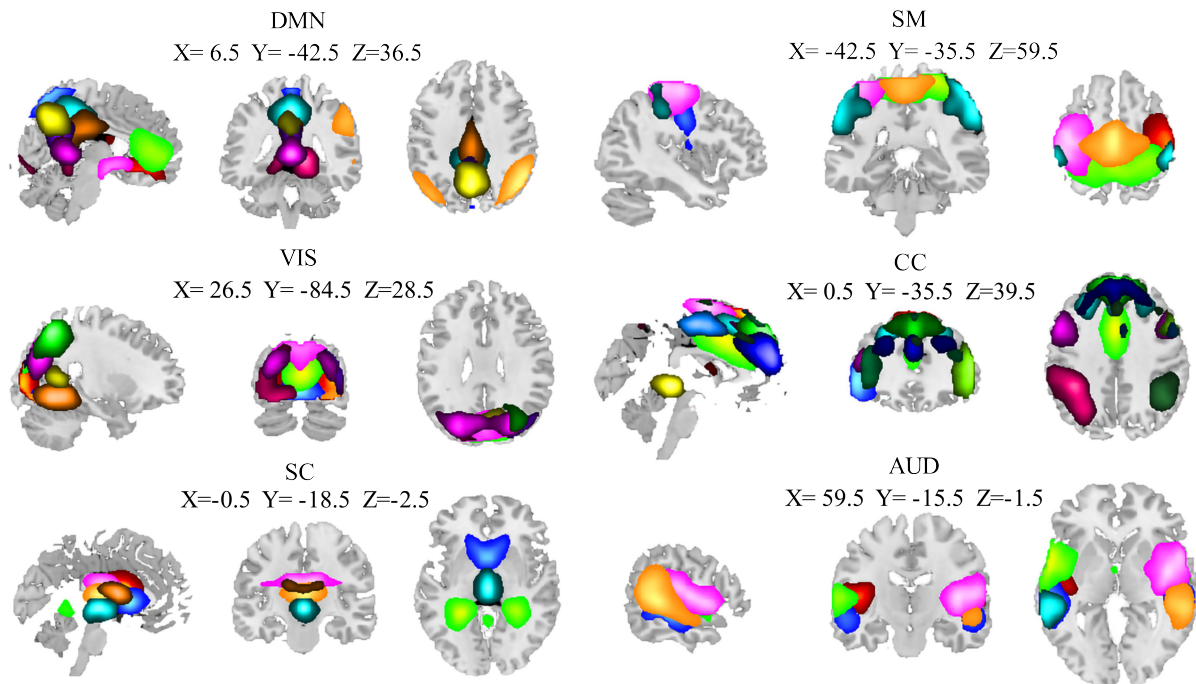
Figure 2. Spatial maps of the 60 independent components result from the entire group (28 elderly and 34 younger adults). The coordinates denote the max peak location of functional domains, and different colors pass spatial information. AUD = auditory domain; CC = cognitive control domain; DMN = default mode domain; SC = subcortical; SM = sensorimotor domain; VIS = visual domain.
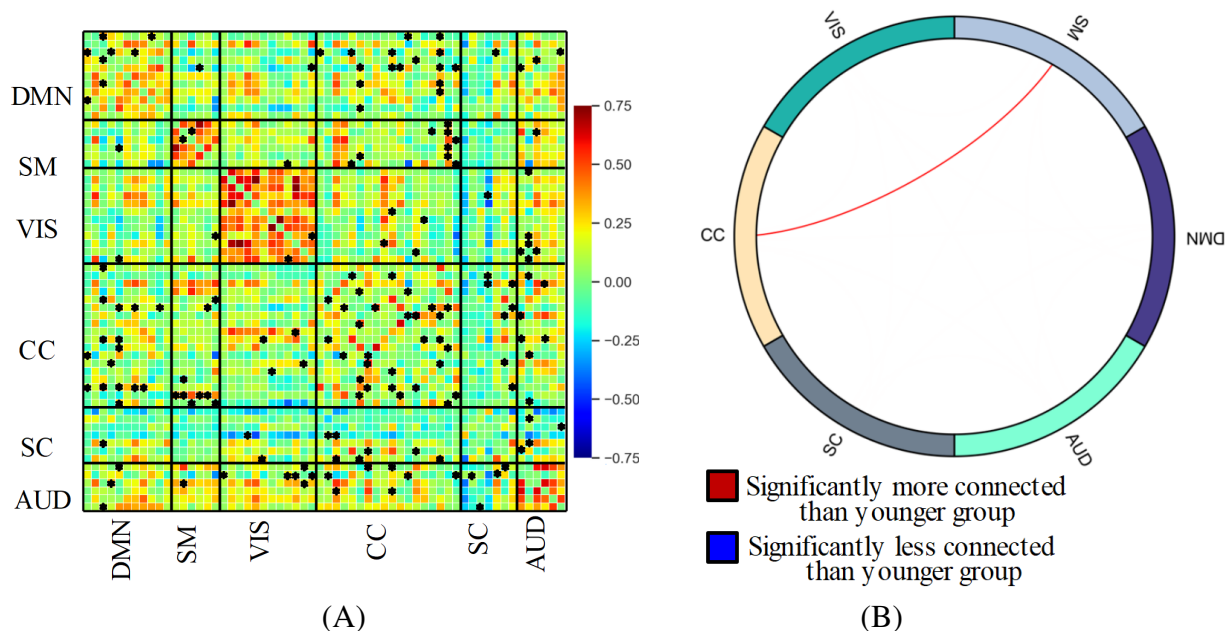

Figure 3. (A) Static functional network connectivity between 60 independent components resulting in 1770 ($60 \times (60-1)/2$)connectivity pairs for the entire group. Asterisks indicate significant differences between the elderly and younger groups. **(B)** Circle plot of significant static functional network connectivity differences of 6 domain between the elderly adult and younger group.

263 3.3 Dynamic functional network connectivity analysis

264 3.3.1 DFNC State

265 Four DFNC states were identified from the clustering. The identified states were the functional patterns
266 that frequently reoccurred across all the participants, and are stable characterisations of the brain activity
267 during the fMRI scanning. The four states are presented in Figure 4(A) indexed with the order given by
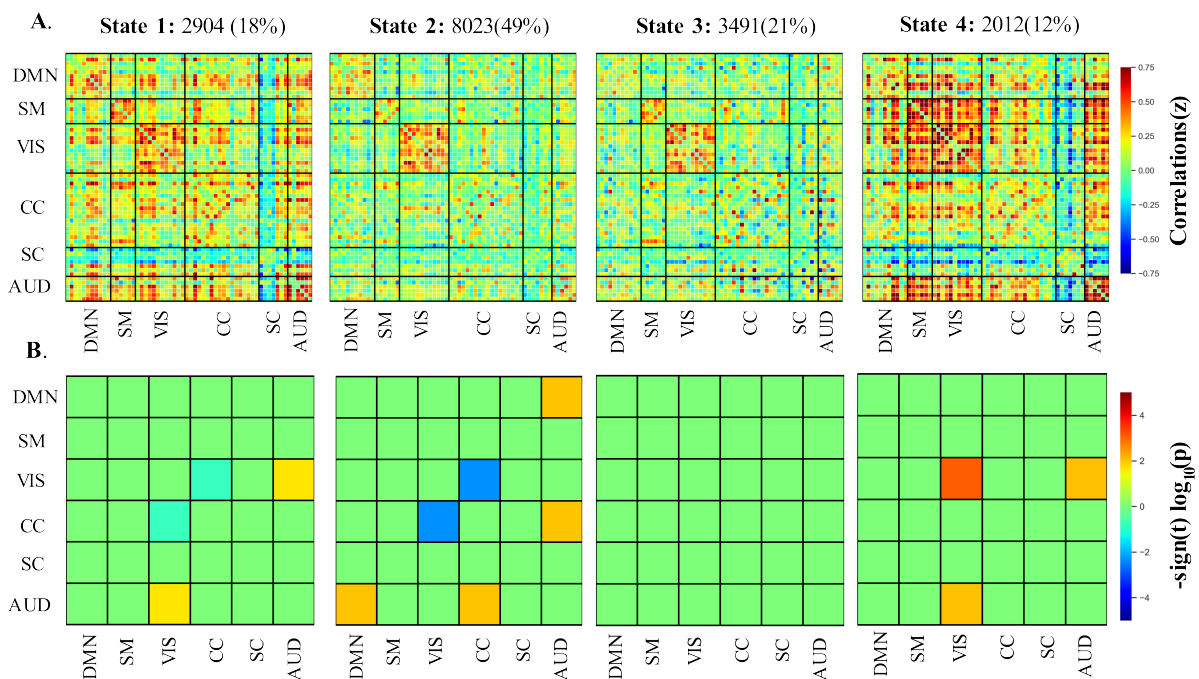268 k-means.

Figure 4. **(A)** 4 functional connectivity states as well as their frequencies across all participants using the group-ICA method. **(B)** Group differences of the 6 selected brain networks between elderly and younger adults in the 4 states. AUD = auditory domain; CC = cognitive control domain; DM = default mode domain; SC = subcortical; SM = sensorimotor domain; VIS = visual domain.

269 According to the connectivity pattern, the states can be grouped into two categories. State 1 and 4
270 compose the first class, characterized by dense inter-and intra-domain connectivity. We can observe highly
271 positive between-AUD domain connectivity and negative between-SC domain connectivity. State 1 closely
272 matches the static connectivity in terms of Manhattan distance. The second category involves states 2 and
273 3. Compared with the first, this class featured relatively weak and sparse connectivity, which is particularly
274 obvious for the SC and AUD domains. Thus, we refer to the category as the weakly connected class. The
275 state frequency of two connectivity types also supports this classification, in which the frequencies of two
276 states in class 1 are no more than 20%, which is less than that of class 2 (which accounts for 70% in total
277 for all subjects). Meanwhile, it is worth noting that the strong positive connectivity within VIS can be
278 observed for all 4 states.

279 Even though the DFNC states exhibit two categories, group differences for each state are varied (see
280 Figure 4(B)). Within state 1, the elderly adults have slightly lower connectivity between VIS and CC while
281 having relatively higher connectivity between VIS and the AUD domain ($p < 0.05$, FDR-corrected). In
282 state 2, the connectivity between VIS and CC in the elder group shows a further decline. At the same time,

283 significantly increased connectivity between DMN and AUD and CC and AUD can be found in this state.
284 The only significantly different intra-domain connectivity was observed in state 4. The result shows that
285 within state 4, the elderly group has markedly stronger connectivity in the VIS domain than younger adults
286 (post t-tests: $p < 0.05$, FDR-corrected). Similar to state 1, the weaker connectivity between VIS and AUD
287 domains can also be observed in state 4. We did not find any significantly different connectivity in state 3
288 between the two groups (post t-tests: $p < 0.05$, FDR-corrected). In contrast to the connectivity difference
289 that the static connectivity state exhibits between the two groups, there is no significant difference between
290 CC and SMN after the FDR-corrected in all 4 states.

3.3.2 DFNC temporal features

292 With four dynamic functional connectivity states and window-based FNC matrices, we subsequently
293 tested for between-group differences in the measures of dynamic features (see Figure 5). Two sample t-tests
294 comparing younger and elderly adults revealed a significant difference in the dynamic measures (fraction
295 and dwell time) of state 2 as well as state 3 (i.e., the weak connectivity pattern, $p < 0.05$, FDR-corrected).
296 In contrast to younger adults, the elderly prefer states 2 and 3 ($p = 0.0001$), and they are more likely to
297 stay in states 2 and 3 once they enter these states ($p = 0.0001$). The between-group difference in dwell
298 time of state 3 is more prominent($p < 0.0001$). No significant between-group difference was observed in
299 terms of the number of state transitions.

300 With respect to the transition probability matrix between states, there were significant between-group
301 effects on the likelihood of staying in one state stably or switch to another. Consistent with the finding that
302 the elderly prefer to spend more time on state 3, results showed that the elderly are more inclined than
303 younger people to switch to state 3 when the current state is not state 3. This is particularly true when the
304 current state is state 2 ($p = 0.0001$, FDR-corrected), demonstrating why the elderly prefer state 2 but have
305 less dwell time than state 3. However, when entering State 3, older people are less likely to remain in this
306 state than younger ones. More elderly people prefer to switch to state 1 or state 2, while younger people
307 tend to maintain a stable state ($p < 0.05$, FDR-corrected). When the next state is state 4, the transition
308 probabilities of elderly and younger people do not differ.

309 To better utilise the dynamic connectivity features to serve ageing classification, we next explored the
310 correlation between these features and the age of participants. The dynamic connectivity features correlated
311 with age have been listed in Table 2. As can be seen, the fraction time and dwell time of state 2 are
312 negatively correlated with age (fraction time: $r = -0.639$, $p = 0.000$; dwell time: $r = -0.502$, $p = 0.000$).
313 In contrast, the fraction time and dwell time of state 3 are positively correlated with age (fraction time:
314 $r = 0.651$, $p = 0.000$; dwell time: $r = 0.555$, $p = 0.000$). In terms of transition probability between states,
315 the likelihood of state 1 switching to state 3, of state 3 switching to state 1, as well as state 3 switching
316 to state 2 all have a positive correlation with age ($r = 0.316, 0.265, 0.254, p = 0.012, 0.038, 0.046$,
317 respectively), while the probability of switching from state 3 to state 3 is negatively correlated with age
318 ($r = -0.409$, $p < 0.001$).

3.3.3 Dynamic graph analysis

320 To explore the age effect on the functional network topology, the subsequent work employed graph
321 theory to characterise the dynamic graph changing during fMRI scanning. Various graph metrics have been
322 utilised, which can describe multiple network properties. These graph measures were calculated based on
323 the sparsing-threshold binary networks per participant and then averaged within the group. Subsequently,
324 they were tested for between-group differences in terms of graph dynamics.
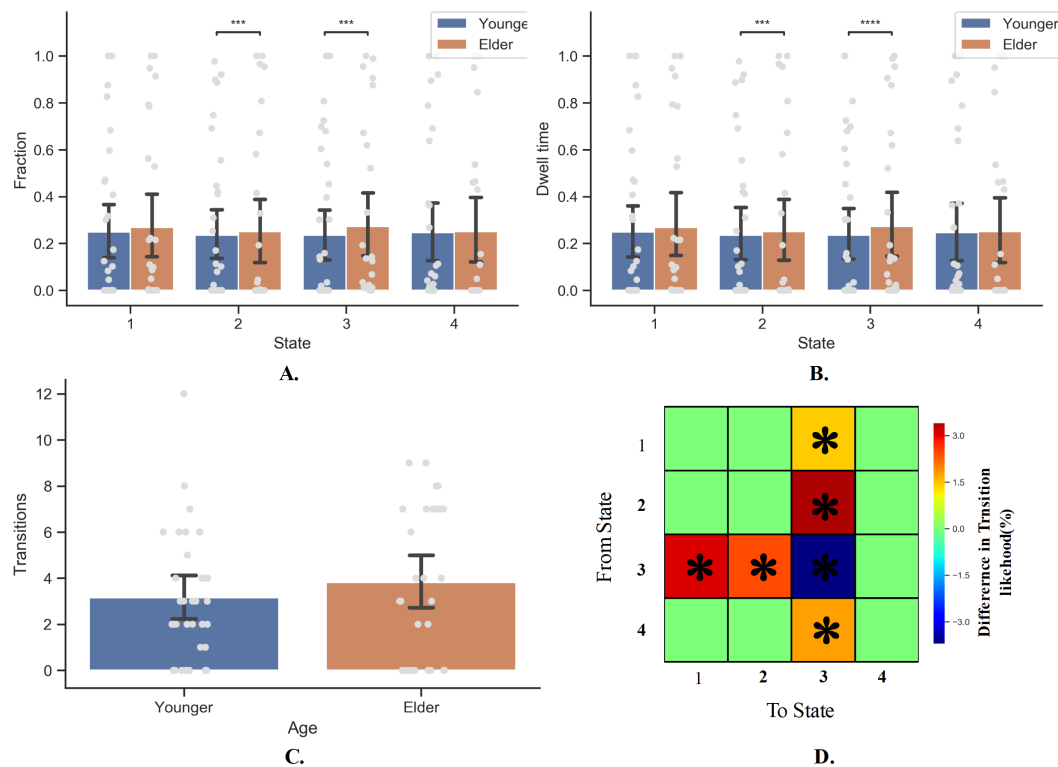
Figure 5. Dynamic connectivity feature analysis for the elderly and younger groups. **(A)** The fraction of time the occurrence of DFC state 2 and state 3 has significant between group difference. The elder prefer state 2 ($P < 0.05$) and state 3($P < 0.05$). **(B)**. The dwell time. Once again, the senior group is more like to stay within state 2 and state 3. **(C)**. The number of transition between states. There is no significant difference in the number of state transition between two groups. **(D)**. State Transition Probability matrix. Comparing with younger adults, the older people more inclined to switch to state 3 when they are in state 1, 2 or 4. However, they are also more likely to transfer to other state when they are entering state 3 than younger people.

Table 2. Dynamic state features correlated with age.

Dynamic Connectivity Features	r	p
Fraction time of State 2	-0.639	0.000
Fraction time of State 3	0.651	0.000
Dwell time of state 2	-0.502	0.000
Dwell time of state 3	0.555	0.000
Transition probability from state 1 to state 3	0.316	0.012
Transition probability from state 3 to state 1	0.265	0.038
Transition probability from state 3 to state 2	0.254	0.046
Transition probability from state 3 to state 3	-0.409	0.001

Firstly, we observed a significant between-group difference in global efficiency ($t = 6.5046$, $p < 0.0001$), local efficiency ($t = -11.4388$, $p < 0.0001$), synchronization ($t = 2.2756$, $p = 0.0232$), hierarchy ($t = 12.384$, $p < 0.0001$), modularity ($t = 16.1638$, $p < 0.0001$), the shortest path ($t = -11.4388$, $p < 0.0001$), clustering coefficient ($t = -4.1766$, $p < 0.0001$) and the betweenness ($t = 10.8943$, $p < 0.0001$). Figure 6 displays the time course of these graph metrics. In terms of efficiency, we can see

Table 3. The correlation between nodal graph measures and age.

r(p<0.05) Metric Domain	Local Efficiency	Vulnerable	Nodal Betwenness
DMN	-0.263	-0.433	-0.496
SMN	0.159	0.2121	0.364
VIS	-0.298	-0.117	0.237
CC	0.048	0.004	0.087
SC	0.252	0.137	-0.093
AUD	0.111	0.049	0.163

330 that the elderly group has a higher global but lower local efficiency than the younger group, suggesting that
331 the information transfer is more efficient in the global but less efficient in the local functional network as
332 age grows. Across these dynamic measures, the elderly people only have three measurements significantly
333 higher than the younger group: the synchronisation coefficient, hierarchy coefficient, and modularity.
334 These higher measures indicate that as the age increases, the synchronisation ability of the functional
335 region in the brain network increases. The raised age increases modularity and enriches the hierarchy
336 structure. Note that the significantly higher value in elderly people is not overwhelming. At some transient
337 time points, these younger people have a stronger performance in these measures. Examples include the
338 weaker synchronisation in the younger group at TR=150, which is consistent with the observed lower
339 synchronisation in transient dynamic state 2 for older adults. A significant difference can also be observed
340 in the clustering coefficient and the shortest path, which directly results in the distinguishing small-world
341 property of the two groups. The lower small-world property implies that the elderly group is less robust to
342 external perturbations, according to the hypothesis by (Barabási, 2013). In that case, it fits our biological
343 intuition that older people are subject to damage by mutation or viral infection. However, there may be a
344 lack of direct evidence to demonstrate a linear relationship.

345   Secondly, there are three other nodal graph measures explored in our work: local efficiency, vulnerable
346 coefficient, and betweenness, which characterise the information-transferring efficiency of a specific
347 node, the vulnerability of a node, and the importance of the node's role in the network, respectively. Six
348 sub-networks were observed to have significant differences between the two groups on the three measures.
349 For the DMN network, people 60 to 80 years old have significantly lower local efficiency($t = -16.8892$,
350 $p < 0.0001$) and vulnerable coefficient ($t = -31.5046$, $p < 0.0001$) than younger people, suggesting
351 the DMN has less efficient information transfer and a higher risk of slowing global efficiency. The same
352 situation occurs in the VIS network ($t = -19.9135$ and -7.0166 for the two metrics, respectively). The
353 DMN network efficiency decline can also be supported by the significantly decreased nodal betweenness (t
354 = -31.8963, p < 0.0001), where the higher the nodal betweenness coefficient, the more likely information
355 will transfer through the node. Figure 7 shows the time-varying curve of these three measures in DMN
356 during the fMRI scan. We can see that older people's metric curves do not have an apparent trend, but they
357 are always lower than younger people's. Besides, the correlation between the nodal graph measures and the
358 age for the six domains also behaved differently (see Table 3). The DMN's local efficiency, vulnerable
359 coefficient, and nodal betweenness have some of the highest negative correlation values compared to the
360 other five networks. On the other hand, the CC domain has the smallest correlation in all three measures
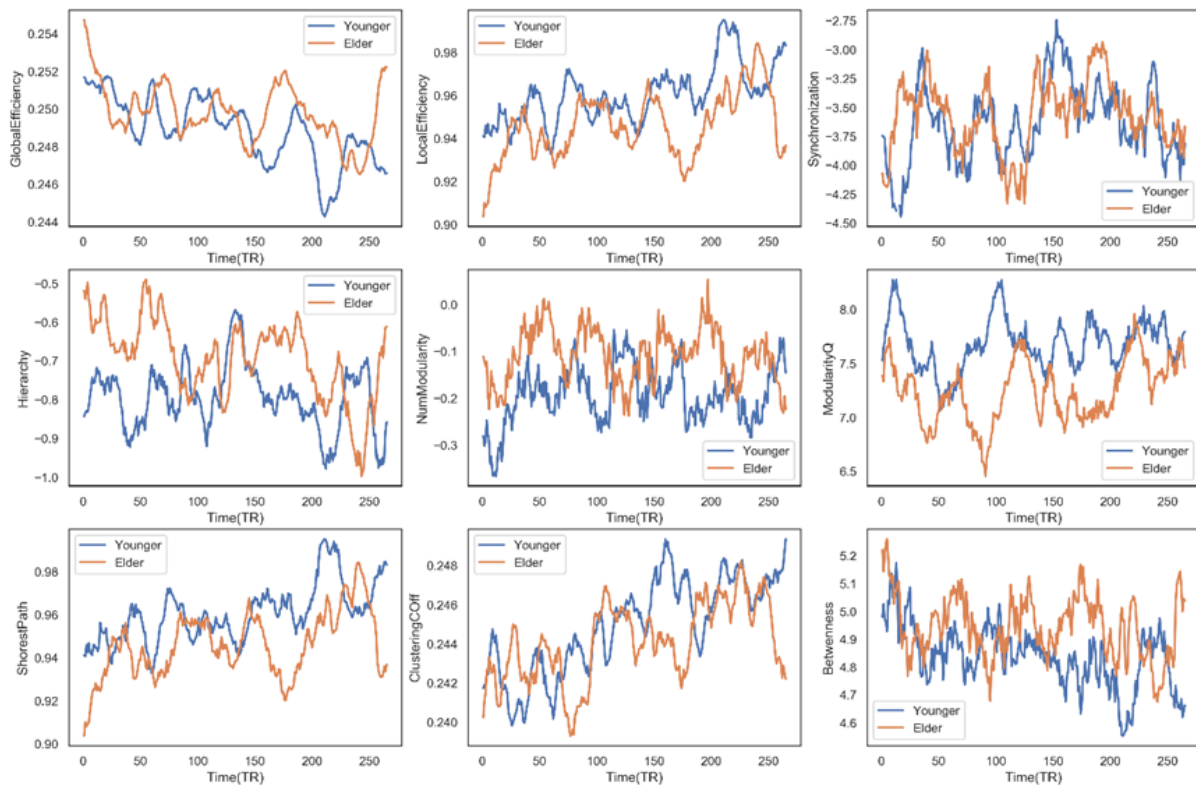361 compared to other parts.

Figure 6. Time course of multiple dynamic measures for the different age groups.
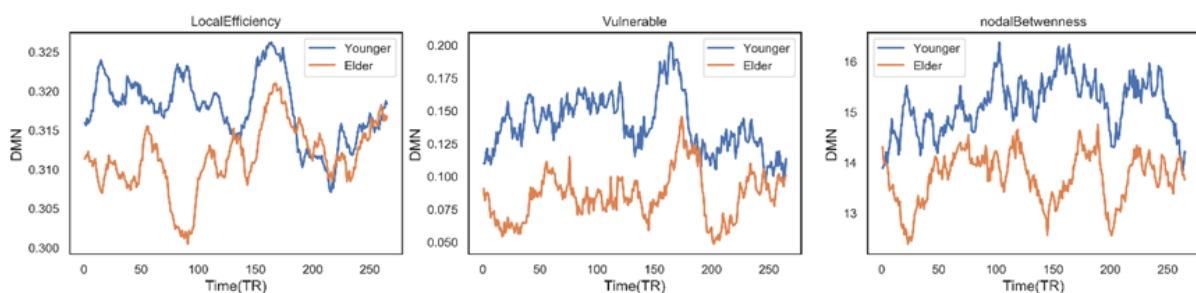

Figure 7. Time varying curve of the three dynamic measures of DMN network: local efficiency, vulnerable, nodal betwenness in age-different group, where no matter which metric elder people are lowest.

3.4 Machine learning test for individual age prediction

Given that the dynamic features are significantly different between the two groups, it is natural to test their power in individual age prediction using a machine learning algorithm.

Firstly, the single dynamic state feature (the fraction, MDT, etc.) was fed into the nine machine learning algorithms respectively to test their prediction power, with the static functional connectivity strength serving as baseline for comparison. The performance of each pipeline was evaluated with 5-fold cross-validation, and the result of the test set is summarized in Table 4. The evaluation metric is accuracy, i.e., the probability that the method correctly categorizes the candidates into the correct class. We report the mean of 5-fold cross-validation results in each metric with a 95% confidence interval.

As can be seen, by using the state fraction feature, all the machine learning algorithms have an accuracy over 80%, which is higher than any other feature (except the AdaBoost method with concatenated

Table 4. The prediction accuracy of multiple machine learning algorithms with dynamic state features. The bold values represent the algorithm that achieves the best performance using the feature indicated in the column. The italic values denote the highest accuracy that the machine learning algorithm could obtain across all the input dynamic features.

| Algorithm | Baseline | Dynamic State Feature | | | | Concatenated |
		Fraction	MDT	NumofTrans.	Transition Probability	
Nearest Neighbors	0.551(0.124)	*0.852 (0.117)*	0.636 (0.251)	0.690 (0.160)	0.648 (0.135)	0.795 (0.200)
Linear SVM	0.531 (0.112)	*0.852 (0.117)*	0.612 (0.152)	0.640 (0.107)	0.648 (0.112)	0.840 (0.124)
RBF SVM	0.531 (0.112)	*0.852 (0.117)*	0.617 (0.207)	0.607 (0.119)	0.631 (0.141)	0.740 (0.186)
Gaussian Process	0.483 (0.106)	*0.838 (0.124)*	0.536 (0.170)	0.690 (0.141)	0.683 (0.1770)	0.729 (0.158)
Decision Tree	0.585 (0.132)	***0.886 (0.129)***	0.583 (0.165)	0.729 (0.175)	0.648 (0.211)	0.840 (0.144)
Random Forest	0.585 (0.153)	*0.855 (0.116)*	**0.650** (0.225)	0.755(0.157)	0.695 (0.175)	0.852 (0.157)
FNN	0.552 (0.173)	*0.838 (0.124)*	0.579 (0.155)	0.560 (0.118)	0.564 (0.104)	0.807 (0.161)
AdaBoost	0.577 (0.111)	0.807 (0.142)	0.617 (0.193)	**0.771** (0.150)	**0.731** (0.195)	***0.855 (0.138)***
Voting	0.511 (0.131)	*0.852 (0.117)*	0.617 (0.193)	0.624 (0.156)	0.679 (0.143)	0.840 (0.163)

feature). The decision tree achieves the highest accuracy of 0.886 using this feature, which is also the best performance in all of the dynamic state features. The highest accuracy for the number of transitions and transition probability is similar, 0.771 and 0.731, respectively. Meanwhile, the best performance of the number of transitions is more stable than that of transition probability, where the accuracy variance is less by 0.04. However, the number of transitions has a large gap in performance in terms of the different methods, where it can only achieve an accuracy of 0.560 with the FNN algorithm. The MDT has the lowest accuracy of 0.650. Concerning the concatenated feature, even though the results are not much worse than those for the number of transitions and transition probability, the highest accuracy is only 0.855, which is still less than the state fraction. On the other hand, with respect to the classic methods, the FNN method is the most unstable one. It obtains a mean accuracy of 0.855 using fractions while it has a 0.560 when using the transition probability as input. For the two ensemble-fusion-strategy-based methods, the voting method did not perform well for individual age prediction, though its best result is still for the fraction feature. In contrast, the AdaBoost method has achieved the best performance three times, the most frequent optimal method.

Second, similar to the dynamic state features, the dynamic graph features were also input into different machine learning algorithms. However, the results were not impressive using the single graph features (see Table 5 and Table 6). All of the features do not achieve accuracy over 70%, the best accuracy was just 0.693 obtained by the SVM with the number of modularity.

4 DISCUSSION

Given the known dynamic nature of brain activity, it is reasonable to use the DFNC method to investigate the differences in dynamics between age groups. In the study presented here, four transient brain states that frequently reoccur at rest were identified. These 4 states exhibit two types of connectivity patterns: the densely inter-and intra-domain connectivity pattern and the weakly sparse one. The elderly tend to transfer to and stay in the weakly connected state, which cannot be shown with static analysis. Notably, the fraction of these DFNC states and the dwell time were correlated with age ($r = 0.6392/0.6507$ for time fraction of state 2 and 3 respectively; $r = 0.5022/0.5553$ for the dwell time of state 2 and 3 respectively). Besides,

Table 5. The prediction accuracy of multiple machine learning algorithms with dynamic graph features (I). The bold values represent the algorithm that achieves the best performance using the feature indicated in the column. The italic values denote the highest accuracy that the machine learning algorithm could obtain across all the input dynamic graph features.

Algorithm	Baseline	Dynamic Graph Feature				
		Global Efficiency	Local Efficiency	Synchronization	Hierarchy	ModularityQ
Nearest Neighbors	0.551 (0.124)	0.5262 (0.208)	0.505 (0.165)	0.481 (0.209)	*0.571* (0.183)	0.533 (0.129)
Linear SVM	0.531 (0.112)	0.555 (0.195)	0.517 (0.142)	0.502 (0.166)	0.506 (0.231)	0.564 (0.220)
RBF SVM	0.531 (0.112)	0.548 (0.066)	0.548 (0.656)	**0.548** (0.066)	0.548 (0.066)	0.548 (0.066)
Gaussian Process	0.483 (0.106)	0.471 (0.271)	0.531 (0.154)	0.469 (0.217)	0.607 (0.141)	***0.617*** (0.111)
Decision Tree	0.585 (0.132)	0.340 (0.155)	**0.567** (0.188)	0.407(0.172)	0.576 (0.172)	0.483 (0.168)
Random Forest	0.585 (0.153)	0.483(0.121)	0.502 (0.157)	0.457 (0.150)	0.579 (0.172)	0.500 (0.226)
FNN	0.552 (0.173)	0.436 (0.161)	0.533 (0.129)	0.467 (0.211)	**0.648** (0.247)	0.483 (0.259)
AdaBoost	0.577 (0.111)	0.505 (0.188)	0.369 (0.228)	0.390 (0.186)	0.569 (0.302)	0.519 (0.209)
Voting	0.511 (0.131)	***0.676*** (0.150)	0.533 (0.217)	0.536 (0.139)	0.500 (0.206)	0.357 (0.129)

Table 6. The prediction accuracy of multiple machine learning algorithms with dynamic state features (II). The bold values represent the algorithm that achieves the best performance using the feature indicated in the column. The italic values denote the highest accuracy that the machine learning algorithm could obtain across all the input dynamic graph features.

Algorithm	Dynamic Graph Feature				Concatenated
	NumModularity	ClusteringCOff	ShorestPath	Betwenness	
Nearest Neighbors	0.562 (0.200)	0.450 (0.171)	0.531 (0.186)	0.529 (0.194)	0.437 (0.049)
Linear SVM	***0.693*** (0.133)	0.486 (0.164)	**0.564** (0.165)	0.500 (0.032)	0.515 (0.074)
RBF SVM	0.548 (0.066)	0.548 (0.066)	0.548 (0.066)	0.548 (0.066)	0.548 (0.019)
Gaussian Process	0.598 (0.123)	0.448 (0.122)	0.500 (0.152)	**0.598** (0.105)	0.548 (0.019)
Decision Tree	*0.579* (0.201)	0.436 (0.143)	0.419 (0.182)	0.567 (0.115)	**0.610** (0.153)
Random Forest	0.517 (0.168)	***0.581*** (0.162)	0.467 (0.189)	0.579 (0.155)	0.421 (0.197)
FNN	*0.662* (0.082)	0.367 (0.149)	0.514 (0.198)	0.550 (0.143)	0.533 (0.012)
AdaBoost	*0.650* (0.121)	0.310 (0.141)	0.507 (0.152)	0.581 (0.207)	0.579 (0.068)
Voting	0.511 (0.222)	0.474 (0.208)	0.529 (0.099)	0.593 (0.188)	0.529 (0.099)

398 these dynamic measures gain advantage in brain age classification compare to static ones. The fraction
399 time of DFNC state can achieve highest accuracy of 0.8857 using a decision tree.

400   There is a significant difference in the dynamic graph topology found between the young group and
401 the elderly group. Older people have higher global but lower local information transformation efficiency,
402 stronger synchronization ability, increased betweenness, more rich modularity and hierarchy structure,
403 shorter shortest path length, and a declining clustering coefficient than younger people. At the nodal
404 level, elderly adults differed from younger people in terms of local efficiency, vulnerable coefficient,
405 and betweenness. The most notable of these differences is that the information transfer efficiency, the
406 vulnerability, and the nodal betweenness of older people's DMN are all less than those of the younger group
407 during the rest period. Thus, we here substantiated the lower role of DMN in elderly people, indicating
408 dynamic analysis's benefit.

4.1 The correlation between dynamic features and mnemonic discrimination ability

Mnemonic discrimination ability (MDA) is the perception ability of humans to distinguish existing memories from current inputs by retrieving and encoding past events or experiences. Studies have shown that the decrease in MDA is a sign of neurodegenerative diseases relative to ageing. Many pieces of evidence show that as age increases, the MDA will significantly decline (Stark et al., 2019, 2013) (Wahlheim et al., 2022). However, whether the relationship is linear or not is not clear.

MDA is usually measured by the lure discrimination index (LDI), calculated as the difference in similar responses to lures and foils in the mnemonic discrimination task (Stark et al., 2019). Previous studies have demonstrated the DMN network has an age-inducted abnormal connectivity (Nash et al., 2021; Raichle, 2015), and this connectivity abnormality can develop a positive prediction model for LDI (Wahlheim et al., 2022). Nevertheless, this prediction is based on the static connectivity strength, the dynamic characteristics of DMN, or broadly, the function sub-networks, have not been thoroughly investigated. Hence, with the LDI provided by the original data source, this section additionally investigates the correlation between age, the dynamic feature, and MDA.

Firstly, age was observed to be negatively correlated with LDI ($r = -0.3890$, $p = 0.001$), which is consistent with the previous findings (Reagh et al., 2016). In terms of dynamic state features, the fraction time of state 2 is positively correlated with LDI ($r = 0.3270$, $p = 0.0094$), and the fraction time of state 3 is negatively correlated with LDI($r = -0.3882$, $p = 0.0018$). Similar to fraction time, the MDT of states 2 and 3 has a significant correlation with LDI, where the correlation is $r = 0.3145$ ($p = 0.0127$) and $r = -0.3591$ ($p = 0.0041$) respectively. There is no significant correlation between the number of transitions and LDI or between transition probability and LDI. Recall that the connectivity pattern of state 3 is both weakly connected. This finding implies that the transient weakly connected state impacts the ability of everyday people to distinguish objects. We speculate the aging brain regulates the fraction of the weak state and its dwell time to determine the perceptive ability. In the weak state, the ability of different brain regions to communicate and coordinate with one another is reduced. As age increases, the brain cannot afford the active connectivity state and prefer a "standby" or "sleep" mode, thus lowering the perceptive function. In addition, cognitive and perceptual changes may be interrelated since they are both susceptible to age-related factors, meaning that a reduction in the functioning of the perceptual system may have an impact on cognitive abilities. Hence, it is possible to speculate that the common finding of cognitive decline in the aging brain could be closely related to the weak state of the brain. However, further experiments are necessary to confirm these speculations and explore the relationship between DFNC differences and health and cognitive function during aging. In addition, compared with state 3, state 2 has obvious positive connectivity within the DMN network, especially between the right angular gyrus and the anterior cingulum, suggesting that the transient state with positive connectivity in the DMN domain may promote the increase of MDA. In fact, previous studies have reported that connections positively related to mnemonic discrimination are broadly distributed across prefrontal, temporal, and parietal regions (Huijbers et al., 2011; Kim, 2016; Sestieri et al., 2011). Thus, we subsequently investigate the correlation between the nodal-level graph measure of DMN and LDI to hopefully extend our understanding of the DMN network's role in MDA.

The results show that only the node betweenness of DMN was observed with a weakly positive correlation ($r = 0.2644$, $p = 0.03780$) among the three nodal graph measures. According to the definition of nodal betweenness, this finding implies that the more information transfer passes through the DMN functional region, the more MDA. Besides, recall the highly negative relationship between DMN nodal betweenness and age. One possible and reasonable reason for the older adults' MDA being significantly lower than

453 younger ones is that the ageing process mitigates DMN participation gradually, thus inducing the decrease
454 in the MDA. However, it may involve a complicated process. To substantiate this implication, more detailed
455 experiments that target the brain DMN function domain are needed.

4.2 Dynamic balance of functional integration and segregation in healthy ageing

457 The brain system keeps normal functions by maintaining the balance of functional integration (of
458 different functional regions' information transmission for function response) and segregation (specialized
459 information processing within the isolated functional regions). In many diseases with psychiatric disorders
460 like schizophrenia, the disrupted balance between segregation and integration within the brain functional
461 network has been demonstrated (Duan et al., 2019; Wang et al., 2016). Previous studies in human ageing
462 also revealed the abnormal integration and segregation within the brain function system: the decreased
463 segregation occurs in the healthy ageing process (Chan et al., 2014; Wig, 2017). Usually, the balance
464 between integration and segregation can be quantified with small-worldness, a graph measure based on
465 the trade-off between high local clustering and short path length (Humphries and Gurney, 2008). This
466 network-level metric measures a graph with many local connections and a few random distance connections.
467 Below, we calculate the dynamic small-worldness to investigate the time-varying balance of integration
468 and segregation.

469 Firstly, the 2-way ANVOA result shows that age has no significant effects on the small-worldness
470 measure ($F = 2.18$, $p = 0.14$), even though this measure is different between transient states. It suggests
471 that the small-world network has not functionally changed as one ages. From the time-varying curve of
472 small-worldness across the entire rest period, we can see that the small-worldness of both young people
473 and the elderly has no clear boundaries. Most of the time, two curves are interwoven together. No one is
474 always higher or lower than another. Besides, the two small-worldness curves are not smooth during the
475 entire rest period. They have large fluctuations, with many spikes. What the spikes mean for the people's
476 behaviors or if their characteristics, like the number of spikes and the energy, cause the age difference has
477 not been clear. However, the measured value always fluctuates around 1 as time goes by, which means that
478 both younger and older people keep a dynamic balance of functional integration and segregation.

479 Subsequently, from other graph metrics, we may have some clues to the changed functional integration
480 and segregation in elderly people. As a spatially isolated functional specialization, segregation has multiple
481 ways to be quantified. For example, previous studies have quantified segregation with the relationship
482 connectivity strength within and between the modules (Bonkhoff et al., 2020; Chan et al., 2014; Wig,
483 2017). Hence, segregation is often connected with brain modularity. The higher the value of modularity, the
484 more segregation in functional domains. Recall the modularity measure curves in Figure 6. The elderly's
485 modularity is nearly always lower than the young, which perhaps implies more functional segregation
486 in senior group people. However, a prior study in a long-term observation has demonstrated that the
487 modularity and segregation might follow a U-shaped curve (Duncan and Small, 2016). Thus, the simple
488 linear relationship between modularity and segregation in terms of age may not be true, and more evidence
489 is needed to support that.

5 CONCLUSION

490 Ageing has a profound influence on brain functional connectivity. This paper employed the DFNC method
491 to explore the altered dynamic brain function interaction using the resting fMRI scans. Compared with
492 static approach, the DNFC can capture the transient brain state in the elderly as well as young adults. The
493 statistical analysis shows that the state-related features are significantly different between senior adults aged

60 to 80 and younger adults aged 18 to 30. In addition, DFNC exhibits the graph topology change spanning the entire scan, suggesting that growing age will induce an alteration in the information transformation efficiency, the robustness of the brain function network, and the dynamic balance of brain integration and segregation. Furthermore, this paper demonstrates that the time fraction of a transient stage could assist in brain age prediction due to the essential clues it carries (with the highest accuracy of 0.88). Overall, using a DFNC approach allows new insights into the systems-level effects that brain ageing has on dynamic neural interaction, highlighting that the human brain tends to form differential function coupling patterns with ageing. In future work, this function pattern alteration would be promising to help us interpret the relationship between aging and elderly-related diseases such as Alzheimer's disease or stroke.

CONFLICT OF INTEREST STATEMENT

The authors declare that the research was conducted in the absence of any commercial or financial relationships that could be construed as a potential conflict of interest.

AUTHOR CONTRIBUTIONS

KC, BJ, KN, QF contributed to the conception and design of the study. KC organized the database, and wrote the first draft of the manuscript. All authors contributed to manuscript revision, read, and approved the submitted version.

FUNDING

ACKNOWLEDGMENTS

SUPPLEMENTAL DATA

The supplemental materials and data can be found in the attached Supplementary Materials.

DATA AVAILABILITY STATEMENT

The datasets analyzed for this study can be found in the OpenNEURO REPOSITORY.

MATLAB scripts for DFNC computation were based on templates available in the GIFT toolbox, additional jupyter notebooks in python 3.7 for statistical evaluations and visualizations can be found here

REFERENCES

Abbott, A. (2011). Dementia: a problem for our age. *Nature* 475, S2–S4

Abrol, A., Rashid, B., Rachakonda, S., Damaraju, E., and Calhoun, V. D. (2017). Schizophrenia shows disrupted links between brain volume and dynamic functional connectivity. *Frontiers in neuroscience* 11, 624

520 Aggarwal, C. C., Hinneburg, A., and Keim, D. A. (2001). On the surprising behavior of distance metrics in
521   high dimensional space. In *International Conference on Database Theory* (Springer), 420–434

522 Allen, E. A., Damaraju, E., Plis, S. M., Erhardt, E. B., Eichele, T., and Calhoun, V. D. (2014). Tracking
523   whole-brain connectivity dynamics in the resting state. *Cerebral Cortex* 24, 663–676

524 Ashburner, J. and Friston, K. J. (2005). Unified segmentation. *Neuroimage* 26, 839–851

525 Barabási, A.-L. (2013). Network science. *Philosophical Transactions of the Royal Society A: Mathematical,*
526   *Physical and Engineering Sciences* 371, 20120375

527 Benjamini, Y. and Hochberg, Y. (1995). Controlling the false discovery rate: a practical and powerful
528   approach to multiple testing. *Journal of the Royal Statistical Society: Series B (Methodological)* 57,
529   289–300

530 Bonkhoff, A. K., Espinoza, F. A., Gazula, H., Vergara, V. M., Hensel, L., Michely, J., et al. (2020).
531   Acute ischaemic stroke alters the brain's preference for distinct dynamic connectivity states. *Brain* 143,
532   1525–1540

533 Calhoun, V. D., Adali, T., Pearlson, G. D., and Pekar, J. J. (2001). A method for making group inferences
534   from functional MRI data using independent component analysis. *Human Brain Mapping* 14, 140–151

535 Calhoun, V. D., Miller, R., Pearlson, G., and Adalı, T. (2014). The chronnectome: time-varying connectivity
536   networks as the next frontier in fMRI data discovery. *Neuron* 84, 262–274

537 Chan, M. Y., Park, D. C., Savalia, N. K., Petersen, S. E., and Wig, G. S. (2014). Decreased segregation of
538   brain systems across the healthy adult lifespan. *Proceedings of the National Academy of Sciences* 111,
539   E4997–E5006

540 Chen, Y., Wang, W., Zhao, X., Sha, M., Liu, Y., Zhang, X., et al. (2017). Age-related decline in the
541   variation of dynamic functional connectivity: a resting state analysis. *Frontiers in Aging Neuroscience* 9,
542   203

543 Cole, J. H., Ritchie, S. J., Bastin, M. E., Hernández, M. V., Maniega, S. M. n., Royle, N., et al. (2018).
544   Brain age predicts mortality. *Molecular Psychiatry* 23, 1385–1392

545 Dennis, E. L. and Thompson, P. M. (2014). Functional brain connectivity using fMRI in aging and
546   Alzheimer's disease. *Neuropsychology Review* 24, 49–62

547 Di, X. and Biswal, B. B. (2015). Dynamic brain functional connectivity modulated by resting-state
548   networks. *Brain Structure and Function* 220, 37–46

549 Duan, J., Xia, M., Womer, F. Y., Chang, M., Yin, Z., Zhou, Q., et al. (2019). Dynamic changes of functional
550   segregation and integration in vulnerability and resilience to schizophrenia. *Human Brain Mapping* 40,
551   2200–2211

552 Duncan, E. S. and Small, S. L. (2016). Increased modularity of resting state networks supports improved
553   narrative production in aphasia recovery. *Brain Connectivity* 6, 524–529

554 Fjell, A. M., Sneve, M. H., Storsve, A. B., Grydeland, H., Yendiki, A., and Walhovd, K. B. (2016). Brain
555   events underlying episodic memory changes in aging: a longitudinal investigation of structural and
556   functional connectivity. *Cerebral Cortex* 26, 1272–1286

557 Geerligs, L., Renken, R. J., Saliasi, E., Maurits, N. M., and Lorist, M. M. (2015). A brain-wide study of
558   age-related changes in functional connectivity. *Cerebral Cortex* 25, 1987–1999

559 Grady, C., Sarraf, S., Saverino, C., and Campbell, K. (2016). Age differences in the functional interactions
560   among the default, frontoparietal control, and dorsal attention networks. *Neurobiology of Aging* 41,
561   159–172

562 Griffanti, L., Douaud, G., Bijsterbosch, J., Evangelisti, S., Alfaro-Almagro, F., Glasser, M. F., et al. (2017).
563   Hand classification of fMRI ICA noise components. *Neuroimage* 154, 188–205

564 Hashmi, J. A., Loggia, M. L., Khan, S., Gao, L., Kim, J., Napadow, V., et al. (2017). Dexmedetomidine
565   disrupts the local and global efficiencies of large-scale brain networks. *Anesthesiology* 126, 419–430

566 Hastie, T., Rosset, S., Zhu, J., and Zou, H. (2009). Multi-class adaboost. *Statistics and its Interface* 2,
567   349–360

568 Himberg, J. and Hyvarinen, A. (2003). ICASSO: software for investigating the reliability of ICA estimates
569   by clustering and visualization. In *IEEE XIII Workshop on Neural Networks for Signal Processing*
570   (IEEE), 259–268

571 Hindriks, R., Adhikari, M. H., Murayama, Y., Ganzetti, M., Mantini, D., Logothetis, N. K., et al.
572   (2016). Can sliding-window correlations reveal dynamic functional connectivity in resting-state fmri?
573   *Neuroimage* 127, 242–256

574 Huijbers, W., Pennartz, C. M., Cabeza, R., and Daselaar, S. M. (2011). The hippocampus is coupled with
575   the default network during memory retrieval but not during memory encoding. *PloS One* 6, e17463

576 Humphries, M. D. and Gurney, K. (2008). Network 'small-world-ness': a quantitative method for
577   determining canonical network equivalence. *PloS One* 3, e0002051

578 Kim, H. (2016). Default network activation during episodic and semantic memory retrieval: a selective
579   meta-analytic comparison. *Neuropsychologia* 80, 35–46

580 Kim, J., Criaud, M., Cho, S. S., Díez-Cirarda, M., Mihaescu, A., Coakeley, S., et al. (2017). Abnormal
581   intrinsic brain functional network dynamics in Parkinson's disease. *Brain* 140, 2955–2967

582 Liégeois, R., Ziegler, E., Phillips, C., Geurts, P., Gómez, F., Bahri, M. A., et al. (2016). Cerebral functional
583   connectivity periodically (de) synchronizes with anatomical constraints. *Brain Structure and fFunction*
584   221, 2985–2997

585 Nash, M. I., Hodges, C. B., Muncy, N. M., and Kirwan, C. B. (2021). Pattern separation beyond the
586   hippocampus: A high-resolution whole-brain investigation of mnemonic discrimination in healthy adults.
587   *Hippocampus* 31, 408–421

588 Power, J. D., Barnes, K. A., Snyder, A. Z., Schlaggar, B. L., and Petersen, S. E. (2012). Spurious but
589   systematic correlations in functional connectivity MRI networks arise from subject motion. *Neuroimage*
590   59, 2142–2154

591 Preti, M. G., Bolton, T. A., and Van De Ville, D. (2017). The dynamic functional connectome: State-of-the-
592   art and perspectives. *Neuroimage* 160, 41–54

593 Raichle, M. E. (2015). The brain's default mode network. *Annual Review of Neuroscience* 38, 433–447

594 Rashid, B., Poole, V. N., Fortenbaugh, F. C., Esterman, M., Milberg, W. P., McGlinchey, R. E., et al. (2021).
595   Association between metabolic syndrome and resting-state functional brain connectivity. *Neurobiology*
596   *of aging* 104, 1–9

597 Reagh, Z. M., Ho, H. D., Leal, S. L., Noche, J. A., Chun, A., Murray, E. A., et al. (2016). Greater loss of
598   object than spatial mnemonic discrimination in aged adults. *Hippocampus* 26, 417–422

599 Reeve, A., Simcox, E., and Turnbull, D. (2014). Ageing and Parkinson's disease: why is advancing age the
600   biggest risk factor? *Ageing Research rReviews* 14, 19–30

601 Ruta, D. and Gabrys, B. (2005). Classifier selection for majority voting. *Information Fusion* 6, 63–81

602 Salman, M. S., Du, Y., Lin, D., Fu, Z., Fedorov, A., Damaraju, E., et al. (2019). Group ICA for identifying
603   biomarkers in schizophrenia: 'adaptive' networks via spatially constrained ICA show more sensitivity to
604   group differences than spatio-temporal regression. *Neuroimage: Clinical* 22, 101747

605 Schaefer, A., Margulies, D. S., Lohmann, G., Gorgolewski, K. J., Smallwood, J., Kiebel, S. J., et al. (2014).
606   Dynamic network participation of functional connectivity hubs assessed by resting-state fMRI. *Frontiers*
607   *in Human Neuroscience* 8, 195

608 Sestieri, C., Corbetta, M., Romani, G. L., and Shulman, G. L. (2011). Episodic memory retrieval, parietal
609 cortex, and the default mode network: functional and topographic analyses. *Journal of Neuroscience* 31,
610 4407–4420

611 Snyder, W., Uddin, L. Q., and Nomi, J. S. (2021). Dynamic functional connectivity profile of the salience
612 network across the life span. *Human Brain Mapping* 42, 4740–4749

613 Stark, S. M., Kirwan, C. B., and Stark, C. E. (2019). Mnemonic similarity task: A tool for assessing
614 hippocampal integrity. *Trends in Cognitive Sciences* 23, 938–951

615 Stark, S. M., Yassa, M. A., Lacy, J. W., and Stark, C. E. (2013). A task to assess behavioral pattern
616 separation (BPS) in humans: Data from healthy aging and mild cognitive impairment. *Neuropsychologia*
617 51, 2442–2449

618 Thomason, M. E., Chang, C. E., Glover, G. H., Gabrieli, J. D., Greicius, M. D., and Gotlib, I. H. (2008).
619 Default-mode function and task-induced deactivation have overlapping brain substrates in children.
620 *Neuroimage* 41, 1493–1503

621 Tu, Y., Fu, Z., Zeng, F., Maleki, N., Lan, L., Li, Z., et al. (2019). Abnormal thalamocortical network
622 dynamics in migraine. *Neurology* 92, e2706–e2716

623 Uddin, L. Q., Nomi, J. S., Hébert-Seropian, B., Ghaziri, J., and Boucher, O. (2017). Structure and
624 function of the human insula. *Journal of Clinical Neurophysiology: Official Publication of the American*
625 *Electroencephalographic Society* 34, 300

626 van den Heuvel, M. P., de Lange, S. C., Zalesky, A., Seguin, C., Yeo, B. T., and Schmidt, R. (2017).
627 Proportional thresholding in resting-state fMRI functional connectivity networks and consequences for
628 patient-control connectome studies: Issues and recommendations. *Neuroimage* 152, 437–449

629 Vidaurre, D., Llera, A., Smith, S. M., and Woolrich, M. W. (2021). Behavioural relevance of spontaneous,
630 transient brain network interactions in fMRI. *Neuroimage* 229, 117713

631 Viviano, R. P., Raz, N., Yuan, P., and Damoiseaux, J. S. (2017). Associations between dynamic functional
632 connectivity and age, metabolic risk, and cognitive performance. *Neurobiology of Aging* 59, 135–143

633 Wahlheim, C. N., Christensen, A. P., Reagh, Z. M., and Cassidy, B. S. (2022). Intrinsic functional
634 connectivity in the default mode network predicts mnemonic discrimination: A connectome-based
635 modeling approach. *Hippocampus* 32, 21–37

636 Wang, Y., Zhong, S., Jia, Y., Sun, Y., Wang, B., Liu, T., et al. (2016). Disrupted resting-state functional
637 connectivity in nonmedicated bipolar disorder. *Radiology* 280, 529–536

638 Whitfield-Gabrieli, S. and Nieto-Castanon, A. (2012). Conn: a functional connectivity toolbox for
639 correlated and anticorrelated brain networks. *Brain Connectivity* 2, 125–141

640 Wig, G. S. (2017). Segregated systems of human brain networks. *Trends in Cognitive Sciences* 21,
641 981–996

642 Xia, Y., Chen, Q., Shi, L., Li, M., Gong, W., Chen, H., et al. (2019). Tracking the dynamic functional
643 connectivity structure of the human brain across the adult lifespan. *Human Brain Mapping* 40, 717–728

644 Yin, D., Liu, W., Zeljic, K., Wang, Z., Lv, Q., Fan, M., et al. (2016). Dissociable changes of frontal and
645 parietal cortices in inherent functional flexibility across the human life span. *Journal of Neuroscience*
646 36, 10060–10074

647 Zhang, J., Wang, J., Wu, Q., Kuang, W., Huang, X., He, Y., et al. (2011). Disrupted brain connectivity
648 networks in drug-naive, first-episode major depressive disorder. *Biological psychiatry* 70, 334–342